Diffraction Study on the Atomic Structure and Phase Separation of Amorphous Ceramics in the Si−(B)−C−N System. 1. Si−C−N Ceramics

Jörg Haug,* Peter Lamparter, Markus Weinmann, and Fritz Aldinger

Max-Planck-Institut für Metallforschung, Heisenbergstrasse 3, D-70569 Stuttgart, Germany

Received January 31, 2003. Revised Manuscript Received August 20, 2003

Amorphous Si−C−N ceramics were produced over a wide range of compositions by thermolysis of structurally different polysilazanes. The structure of the as-thermolyzed amorphous ceramics and of ceramic samples after additional heat treatments was investigated by diffraction experiments in the wide-angle and the small-angle scattering regimes. Adopting contrast variation by combination of X-rays and neutrons and isotopic substitution, the observed correlations were assigned to individual atomic pairs. The atomic distances found in the ceramics correspond well with the distances in graphite and α-Si_3N_4. Using the concentration contrast method it could be shown quantitatively that the amorphous Si−C−N ceramics consist of an amorphous graphite-like phase and of amorphous $Si_{3+(1/4)x}N_{4-x}C_x$ ($x = 0-4$). The partial pair correlation functions of the two phases could be evaluated. The size of the phase-separated regions, of the order of 10 Å in the as-thermolyzed ceramics, as determined from small-angle scattering, increases upon annealing up to some 10 Å. The partial structure factor of the amorphous carbon phase was simulated by a model. The simulation shows that the atomic arrangement of the amorphous carbon phase in Si−C−N ceramics in the layers is similar to that of glassy carbon, but the order between the layers is less pronounced. With increasing temperature the arrangement of the layers approaches the order in glassy carbon. A sputter-deposited Si−C−N ceramic shows similar short-range order, but no phase separation on a medium-range scale, as compared with precursor-derived ceramics.

1. Introduction

Novel ceramic materials play a major role for new technical applications. Non-oxide ceramic materials are of special interest because of their covalent bonding providing mechanical reliability and high-temperature stability. In recent years, polymer thermolysis became of increasing interest for the synthesis of these new inorganic materials.[1−6] For the synthesis of Si−C−N ceramics usually polysilazanes[7−12] and polysilylcarbodiimides[13−15] are used as polymeric-precursors. The

* Corresponding author: Jörg Haug, Hahn Meitner Institut Berlin, Glienicker Strasse 100, D-14109 Berlin, Germany. E-mail: haug@hmi.de.

(1) (a) Wills, R. R.; Markle, R. A.; Mukherjee, S. P. *Am. Ceram. Soc. Bull.* **1983**, *62*, 905. (b) Yajima, S. *Am. Ceram. Soc. Bull.* **1983**, *62*, 893. (c) Laine, R. M. *Transformation of Organometallics into Common and Exotic Materials: Design and Activation*; Proceedings of the NATO Advanced Research Workshop, Cap D'Agde, France, 1986. (d) Segal, D. *Chemical Synthesis of Advanced Ceramic Materials*; Cambridge University Press, New York, 1987. (e) Zeldin, M., Wynne, K. J., Allcock H. R., Eds. *Inorganic and Organometallic Polymers, Advanced Materials and Intermediates*; ACS Symposium Series 360; American Chemical Society: Washington, DC, 1988. (f) Wisian-Neilson, P., Allcock, H. R., Wynne, K. J., Eds. *Inorganic and Organometallic Polymers II, Advanced Materials and Intermediates*; ACS Symposium Series 572; American Chemical Society: Washington, DC, 1994.

(2) (a) Peuckert, M.; Vaahs, T.; Brück, M. *Adv. Mater.* **1990**, *2*, 398. (b) Toreki, W. *Polym. News* **1991**, *16*, 6. (c) Birot, M.; Pillot, J.-P.; Dunoguès, J. *Chem. Rev.* **1995**, *95*, 1443.

(3) (a) Bill, J.; Aldinger, F. *Adv. Mater.* **1995**, *7*, 775. (b) Bill, J.; Aldinger, F. *Z. Metallk.* **1996**, *87*, 827. (c) Bill, J., Wakai, F., Aldinger, F., Eds. *Precursor-Derived Ceramics*; Wiley-VCH: Weinheim, Germany, 1999.

(4) (a) Laine, R. M.; Babonneau, F. *Chem. Mater.* **1993**, *5*, 260. (b) Richter, R.; Roewer, G.; Böhme, U.; Busch, K.; Babonneau, F.; Martin, H. P.; Müller, E. *Appl. Organomet. Chem.* **1997**, *11*, 71. (c) Roewer, G.; Herzog, U.; Trommer, K.; Müller. E.; Frühauf, S. *Struct. Bonding* **2002**, *101*, 59.

(5) (a) Weinmann, M.; Aldinger, F. In *Handbook of Advanced Ceramics*, Somiya, S., et al., Eds.; Elsevier: New York, 2003; pp 267−370. (b) Riedel, R. In *Materials Science and Technology;* Cahn, R. W., Haasen, P., Kramer E. J., Eds.; VCH: Weinheim, Germany, 1996; p 1, Chapter 11, Advanced Ceramics from Inorganic Polymers.

(6) Baldus, H.; Jansen, M. *Angew. Chem., Int. Ed. Engl.* **1997**, *36*, 328.

(7) For selected reviews see: (a) Laine, R. M.; Sellinger, A. In *The Chemistry of Organic Silicon Compounds*; Rappoport, Z., Apeloig, Y., Eds; J. Wiley & Sons: London, 1998; Vol. 2. (b) Kroke, E.; Li, Y.-L.; Konetschny, C.; Lecomte, E.; Fasel, C.; Riedel, R. *Mater. Sci. Eng.* **2000**, *R26*, 97.

(8) Rochow, E. G. *Pure Appl. Chem.* **1966**, *13*, 247.

(9) Andrianov, K. A.; Kotrelev, G. V. *J. Organomet. Chem.* **1967**, *7*, 217.

(10) (a) Verbeek, W. Ger. Offen DE 2 218 960, 1973. (b) Verbeek, W.; Winter, G. Ger. Offen DE 2 236 068, 1974.

(11) (a) Seyferth, D.; Wiseman, G. H.; Prud'homme, C. *J. Am. Ceram. Soc.* **1983**, *66*, C-13. (b) Seyferth, D.; Wiseman, G. H.; Prud'homme, C. *Mater. Sci. Res.* **1984**, *17*, 263. (c) Seyferth, D.; Wiseman, G. H. *Polym. Prepr. (Am. Chem. Soc., Div. Polym. Chem.)* **1984**, *25*, 10.

(12) (a) Lavedrine, A.; Bahloul, D.; Goursat, P.; Choong Kwet Yive, N. S.; Corriu, R. J. P.; Leclercq, D.; Mutin, P. H.; Vioux, A. *J. Eur. Ceram. Soc.* **1991**, *8*, 221. (b) Choong Kwet Yive, N. S.; Corriu, R. J. P.; Leclercq, D.; Mutin, P. H.; Vioux, A. *New J. Chem.* **1991**, *15*, 85. (c) Choong Kwet Yive, N. S.; Corriu, R. J. P.; Leclercq, D.; Mutin, P. H.; Vioux, A. *Chem. Mater.* **1992**, *4*, 141. (d) Bahloul, D.; Pereira, M.; Goursat, P.; Choong Kwet Yive, N. S.; Corriu, R. J. P. *J. Am. Ceram. Soc.* **1993**, *76*, 1156.

(13) (a) Ebsworth, E. A.; Mays, M. J. *J. Chem. Soc.* **1961**, 4879. (b) Ebsworth, E. A.; Mays, M. *J. Angew. Chem.* **1962**, *74*, 117.

(14) (a) Pump, J.; Wannagat, U. *Angew. Chem.* **1962**, *74*, 117. (b) Pump, J.; Wannagat, U. *Ann. Chem.* **1962**, *652*, 21. (c) Pump, J.; Rochow, E. G.; Wannagat, U. *Monatsh. Chem.* **1963**, *94*, 588. (d) Pump, J.; Rochow, E. G. *Z. Anorg. Allg. Chem.* **1964**, *330*, 101.

10.1021/cm031029f CCC: $27.50
Published on Web 12/11/2003

structure of the precursor-derived ceramics after thermolysis is predominantly amorphous and transforms into crystalline phases after treatment at high temperatures.[16−18] The advantages of these precursor-derived ceramics, as compared to ceramics obtained by conventional methods such as sintering, are high chemical purity, low processing temperatures, and the absence of sinter additives. A further advantage is the possibility to produce fibers, coatings, infiltration, and bulk parts in an easy manner.

For a better understanding of properties of precursor-derived ceramics, detailed information about the structure of the amorphous state is required. Such information can be obtained, for example, by means of IR and NMR spectroscopy, X-ray and neutron diffraction, or electron microscopy.

The existence of mixed $Si(C,N)_4$ tetrahedra and a free carbon phase in ternary amorphous Si−C−N ceramics has been concluded from neutron diffraction.[19] A detailed study on $Si_{24}C_{43}N_{33}$, derived from a polysilylcarbodiimide precursor,[20,21] combining diffraction in the wide-angle as well as in the small-angle regime and adopting contrast variation by X-ray and neutron diffraction and by ^{nat}N -^{15}N isotopic substitution, revealed that this ceramic, which lies on the C−Si_3N_4 tie-line, is phase separated into two amorphous phases: amorphous carbon and amorphous Si_3N_4. The extension of the separated regions in the as-thermolyzed (at 1100 °C) ceramic was found to be of the order of 20 Å which increased upon annealing at 1400 °C up to 40 Å. In a combined X-ray and neutron diffraction study on a $Si_{40}C_{24}N_{36}$ ceramic, derived from a polyhydromethylsilazane precursor,[22] which lies apart from the C−Si_3N_4 tie-line (N/Si < 4:3), in addition to Si−N bonds Si−C bonds were also detected.

An investigation of the influence of the type of precursor on the medium-range structure of Si−C−N ceramics by X-ray and neutron small-angle scattering[23] showed that all thermolyzed ceramics, independently of the specific precursor, were phase separated into a Si_3N_4-like phase and a free carbon phase on a microscale of the order of some 10 Å which coarsened upon further annealing.

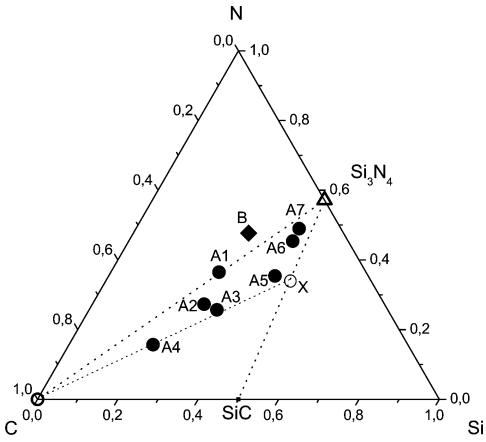

Figure 1. Si−C−N phase diagram indicating the compositions of the investigated Si−C−N ceramics: A, precursor-derived; B, sputtered. Amorphous Si_3N_4 (△) and glassy carbon (○) are included. For the composition X see text.

Structural investigations of as-thermolyzed Si−C−N ceramics by means of solid state ^{29}Si NMR spectroscopy pointed out that silicon is 4-fold coordinated by carbon and nitrogen.[24−28] Very broad resonance signals, centered at around −20 to −30 ppm, suggested the presence of a mixture of SiC_3N, SiC_2N_2, $SiCN_3$, and $SiCN_4$ sites. Depending on the chemical composition, phase separation into Si_3N_4 and/or SiC was observed at around 1450−1550 °C, whereas from thermogravimetric analysis (TGA) there was no hint for decomposition reactions between 800 and 1400 °C.

In the present research project, the short-range and the intermediate-range structures of various amorphous ceramics from the Si−B−C−N system were investigated by X-ray and neutron scattering experiments. The present paper (Part I) reports the results for the ternary Si−C−N ceramics. For these ceramics the study presents a continuation of previous studies[20−22] (which have been focused on a single ceramic each) with the aim to investigate the structure of the ceramics over a wide range of chemical composition (see Figure 1) and to separate the structural functions, as obtained by diffraction, quantitatively into the partial contributions of the two constituting phases, amorphous Si_3N_4 and

(15) (a) Kienzle, A.; Obermeyer, A.; Riedel, R.; Aldinger, F.; Simon, A. *Chem. Ber.* **1993**, *126*, 2569. (b) Obermeyer, A.; Kienzle, A.; Weidlein, J.; Riedel, R.; Simon, A. *Z. Anorg. Allg. Chem.* **1994**, *620*, 1357. (c) Gabriel, A. O.; Riedel, R. *Angew. Chem., Int. Ed. Engl.* **1997**, *36*, 384. (d) Gabriel, A. O.; Riedel, R.; Storck, S.; Maier, W. F. *Appl. Organomet. Chem.* **1997**, *11*, 833. (e) Riedel, R.; Kroke, E.; Greiner, A.; Gabriel, A. O.; Ruwisch, L.; Nicolich, J. *Chem. Mater.* **1998**, *19*, 2964. (f) Riedel, R.; Gabriel, A. O. *Adv. Mater.* **1999**, *11*, 207. (g) Riedel, R.; Greiner, A.; Miehe, G.; Dressler, W.; Fuess, H.; Bill, J.; Aldinger, F. *Angew. Chem., Int. Ed. Engl.* **1997**, *36*, 603.

(16) Bahloul, D.; Pereira, M.; Goursat, P. *J. Am. Ceram. Soc.* **1993**, *76*, 1156−1162.

(17) Kleebe, H. J.; Suttor, D.; Muller, H.; Ziegler, G. *J. Am. Ceram. Soc.* **1998**, *81*, 2971.

(18) (a) Weinmann, M.; Schuhmacher, J.; Kummer, H.; Prinz, S.; Peng, J.; Seifert, H. J.; Christ, M.; Müller, K.; Bill, J.; Aldinger, F. *Chem. Mater.* **2000**, *12*, 623. (b) Müller, A.; Gerstel, P.; Weinmann, M.; Bill, J.; Aldinger, F. *J. Eur. Ceram. Soc.* **2000**, *20*, 2655. (c) Weinmann, M.; Nast, S.; Berger, F.; Müller, K.; Aldinger, F. *Appl. Organomet. Chem.* **2001**, *15*, 867. (d) Janakiraman, N.; Weinmann, M.; Aldinger, F.; Schuhmacher, J.; Bill, J.; Singh, P. *J. Am. Ceram. Soc.* **2002**, *85*, 1807.

(19) Dixmier, J.; Bellissent, R.; Bahloul, D.; Goursat, P. *J. Eur. Ceram. Soc.* **1994**, *13*, 293.

(20) (a) Dürr, J. *Struktur von amorphen Siliziumcarbonitrid-Keramiken mit Hilfe von Röntgen- und Neutronenstreuuntersuchungen und Isotopensubstitution,* Ph.D. Thesis, Universität Stuttgart, Germany, 1997. (b) Dürr, J.; Lamparter, P.; Bill, J.; Steeb, S. Aldinger, F.; *J. Non-Cryst. Solids* **1998**, *232−234*, 155.

(21) Dürr, J.; Schempp, S.; Lamparter, P.; Bill, J.; Steeb, S.; Aldinger, F. *XIIIth Int. Symp. on the Reactivity of Solids, Hamburg, Sept. 8−12, 1996, Solid State Ionics* **1997**, *101−103*, 1041.

(22) Schempp, S.; Dürr, J.; Lamparter, P.; Bill, J.; Aldinger, F. *Z. Naturforsch.* **1998**, *53a*, 127.

(23) (a) Schempp. S. *Untersuchung des Relaxationsverhaltens amorpher Si−C−N Keramiken bei thermischer Behandlung mit Hilfe der Röntgen- und Neutronenkleinwinkelstreuung,* Ph.D. Thesis, Universität Stuttgart, Germany, 1998. (b) Schempp, S.; Lamparter, P.; Bill, J.; Aldinger, F. *Proceedings of the Werkstoffwoche München, Germany, 1998*; Wiley-VCH: Weinheim, Germany, 1999; p 327.

(24) (a) Dando, N. R.; Perrotta, A. J., Strohmann, C.; Steward, R. M.; Seyferth, D. *Chem. Mater.* **1993**, *5*, 1624. (b) Laine, R. M.; Babonneau, F.; Blowhowiak, K. Y.; Kennish, R. A.; Rahn, J. A.; Exarhos, G. J.; Waldner, K. *J. Am. Ceram. Soc.* **1995**, *78*, 137.

(25) (a) Gérardin, C. M.; Taulelle, F.; Livage, J. *Mater. Res. Soc. Symp. Proc.* **1993**, *287*, 233. (b) Mocaer, D.; Pailler, R.; Naslain, R.; Richard, C.; Pillot, J. P.; Dunogues, J.; Gérardin, C. M.; Taullele, F. *J. Mater. Sci.* **1993**, *28*, 2615. (c) Gérardin, C. M.; Taulelle, F.; Bahloul, D. *J. Mater. Chem.* **1997**, *7*, 117.

(26) El Kortobi, Y.; Sfihi. H.; Legrand, A. P.; Musset, E.; Herlin, N.; Cauchetier, M. *Colloids Surf., A* **1996**, *115*, 319.

(27) Suttor, D.; Hacker, J.; Trassl, S.; Müller, H.; Kleebe, H.-J.; Ziegler, G. *Ceram. Eng. Sci. Proc.* **1997**, *18*, 127. (g) Trassl, S.; Suttor, D.; Motz, G.; Rössler, E.; Ziegler, G. *J. Eur. Ceram. Soc.* **2000**, *20*, 215.

(28) Iwamoto, Y.; Völger, W.; Kroke, E.; Riedel, R.; Saitou, T.; Matsunaga, K. *J. Am. Ceram. Soc.* **2001**, *84*, 2170.

amorphous carbon. In particular, the short-range order of the (graphite-like[20]) carbon phase, and its development upon annealing, was investigated in detail, including the adoption of an existing structural model.

Ceramics were obtained from differently substituted polysilazanes or polysilsesquiazanes or copolymers thereof. $[(H_2C{=}CH)Si(NH)_{1.5}]_n$ and $[(H_2SiNH)_3((H_3C)SiHNH)]_n$ were chosen to produce ceramics with compositions along the tie-line $C-Si_3N_4$ and Si_3N_4-SiC, respectively. Whereas $[(H_2SiNH)_3((H_3C)SiHNH)]_n$ releases only hydrogen during thermolysis, the nitrogen-rich silsesquiazane loses predominantly nitrogen besides hydrogen, until an elemental composition on the tie-line is reached. Ceramic materials with compositions in the three-phase field $C/Si_3N_4/SiC$ were received from $[(H_5C_6)Si(CH_3)NH]_n$, $[(H_2C{=}CH)Si(CH_3)NH]_n$, $[(HSi(NH)_{1.5})((H_3C)Si(NH)_{1.5})_{1.76}]_n$, and $[(HSi(NH)_{1.5})((H_3C)Si(NH)_{1.5})_{0.44}]_n$, whereby the amount of carbon in the thermolyzed materials decreased in the mentioned row. The decreasing amount of carbon is directly related to the carbon content of the silicon-bonded substituents (C_6H_5, $H_2C{=}CH$, CH_3). For contrast variation, ^{15}N-pure $[(H_2C{=}CH)Si(CH_3)\cdot{}^{15}NH]_n$ was synthesized and thermolyzed. In addition, a sputtered Si−C−N ceramic was produced to investigate differences in the structure depending on the manufacturing process of such ceramics. For further details of the present study see ref 29.

The results for the quarternary Si−B−C−N ceramics are reported in the following paper (Part II).

2. Theoretical Background

In the following the essential definitions adopted in the present work are briefly summarized. For more details we refer to the review.[30]

2.1. Atomic Short-Range Order and Wide-Angle Scattering. From the coherently scattered intensity (per atom) $I_{coh}(q)$ the total structure factor $S(q)$ according to Faber and Ziman[31] is obtained

$$S(q) = \frac{I_{coh}(q) - [\langle f^2(q)\rangle - \langle f(q)\rangle^2]}{\langle f(q)\rangle^2} \quad (1)$$

where $I_{coh}(q)$ is coherently scattered intensity per atom; $\langle f^2(q)\rangle = \sum_{i=1}^{n} c_i \cdot f_i^2(q)$; $\langle f(q)\rangle = \sum_{i=1}^{n} c_i \cdot f_i(q)$; c_i is atomic concentration of atomic species i; $f_i(q)$ is scattering length of atomic species i; n is the number of atomic species in the sample; $q = 4\pi\sin\theta/\lambda$ is modulus of the scattering vector; 2θ is the diffraction angle; and λ is wavelength of radiation.

The total pair correlation function $G(r)$, describing the distribution of neighboring atoms around a central atom, is obtained by Fourier transformation of the structure factor $S(q)$ as follows:

$$G(r) = 4\pi r(\rho(r) - \rho_0) = \frac{2}{\pi}\int_0^\infty q[S(q) - 1]\sin(qr)dq \quad (2)$$

where r is the atomic distance; ρ_0 is average atomic density; and $\rho(r)$ is the pair density distribution function.

The radial distribution function $RDF(r)$ is given by

$$RDF(r) = 4\pi r^2\rho(r) \quad (3)$$

The total structure factor $S(q)$ of a system with n components is the weighted sum of $n(n+1)/2$ partial structure factors $S_{ij}(q)$ as follows:

$$S(q) = \frac{1}{\langle f(q)\rangle^2}\cdot\sum_{i=1}^{n}\sum_{j=1}^{n} c_i c_j f_i(q) f_j(q)\cdot S_{ij}(q) = \sum_{i=1}^{n}\sum_{j=1}^{n} W_{ij}(q)\cdot S_{ij}(q) \quad (4)$$

The partial pair correlation functions $G_{ij}(r)$ are related to the partial structure factors $S_{ij}(q)$ according to eq 2. In case of a ternary system ($n = 3$) six partial $G_{ij}(r)$ functions are needed for the structural description of the system ($G_{ij}(r) = G_{ji}(r)$). This would require six independent diffraction experiments where the weighting factors W_{ij} are different by adopting contrast variation methods. Contrast variation can be achieved, e.g., by combination of X-ray and neutron diffraction or by neutron diffraction with isotopic substitution. Because six independent experiments are usually not possible, additional information is needed to evaluate measured total $G(r)$-functions, e.g., by considering atomic distances known from relevant crystalline phases and using peak fitting routines to resolve overlapping peaks.

2.2. Inhomogeneous Structure and Small-Angle Scattering. If a sample is not homogeneous, but contains fluctuations of the composition and/or density on a medium-range scale a small-angle scattering effect may be observed.[32−34] In case of the separation of a phase (regions) p with volume fraction v_1 within a matrix m from the coherently scattered intensity (per volume) $I_{coh}(q)$ two fundamental properties of these regions can be derived.

The dimension of the scattering regions can be determined by the investigation of the Guinier range[32] where the coherently scattered intensity $I_{coh}(q)$ is approximated by the following:

$$I_{coh}(q) = I_{coh}(0)\cdot\exp\left(-\frac{R_G^2}{3}\cdot q^2\right) \quad (5)$$

R_G is the so-called Guinier radius of the scattering regions. For spherical regions it is related to the diameter by $D = 2\cdot\sqrt{5/3}\cdot R_G$.

Further information about the scattering objects can be derived from the so-called invariant Q which is independent of the morphology of the regions:

$$Q = \int_0^\infty q^2\cdot I_{coh}(q)dq = 2\pi^2\cdot v_1\cdot(1 - v_1)\cdot(\Delta\eta)^2 \quad (6)$$

(29) Haug, J. *Untersuchung der Struktur und des Kristallisationsverhaltens von Si−C−N− und Si−B−C−N−Precursorkeramiken mit Röntgen- und Neutronenbeugung*, Ph.D. Thesis, Universität Stuttgart, Germany, 2002.

(30) Lamparter, P.; Steeb, S. In *Materials Science and Technology - A Comprehensive Treatment*; Cahn, R.W., Haasen, P., Kramer, E.J., Eds.; Vol. 1 of *Structure of Solids*; VCH: Weinheim, Germany, 1993; p 218.

(31) Faber, T.; Ziman, *J. Philos. Mag.* **1965**, *11*, 153.

(32) Guinier, A.; Fournet, G. *Small-Angle Scattering of X-rays*; John Wiley & Sons: New York, 1955.

(33) Feigin, L.; Svergun, D. *Structure Analysis by Small-Angle X-ray and Neutron Scattering*; Plenum Press: New York, 1987; Vol. VIII.

(34) Glatter, O., Kratky, O., Eds. *Small Angle X-ray Scattering*; Academic Press Inc.: London, 1982; Vol. X.

Table 1. Synthesis of the Polymeric Precursors for Ceramics A1−A7 and for a-Si_3N_4

	starting compounds; amount of silane, solvent	polymer yield	ceram. yield (%)	ref.
A1	$(H_2C{=}CH)SiCl_3$, NH_3 105 g (650 mmol); 1.5l THF	$[(H_2C{=}CH)Si(NH)_{1.5}]_n$ 41.3 g (530 mmol) 82%	84	35
A2	$(H_2C{=}CH)Si(CH_3)Cl_2$, NH_3 137 g (970 mmol); 1.5l THF	$[(H_2C{=}CH)Si(CH_3)NH]_n$ 70 g (825 mmol) 90%	20	36
A3	$(H_2C{=}CH)Si(CH_3)Cl_2$, $^{15}NH_3$ 42.3 g (300 mmol); 800 mL THF	$[(H_2C{=}CH)Si(CH_3)^{15}NH]_n$ 23.2 g (270 mmol) 90%	*a*	
A4	$(H_5C_6)Si(CH_3)Cl_2$, NH_3 30 g (157 mmol); 500 mL THF	$[(H_5C_6)Si(CH_3)NH]_n$ 19.5 g (144 mmol) 92%	10	36
A5	$HSiCl_3 + (H_3C)SiHCl_2$, NH_3 20 g (150 mmol) + 33 g (286 mmol); 800 mL THF	$[(HSi(NH)_{1.5})((H_3C)SiH{-}NH)_{1.9}]_n$ 22 g (134 mmol) 89%	74	
A6	$HSiCl_3 + (H_3C)SiHCl_2$, NH_3 40 g (295 mmol) + 16 g (140 mmol); 800 mL THF	$[(HSi(NH)_{1.5})((H_3C)SiH{-}NH)_{0.47}]_n$ 22 g (130 mmol) 93%	85	
A7	$3\ H_2SiCl_2 + (H_3C)SiHCl_2$, NH_3 35 g (350 mmol) + 13.3 g (117 mmol); 800 mL THF	$[(H_2SiNH)_3((H_3C)SiH{-}NH)]_n$ 22.3 g (130 mmol) 99%	94	*b*
a-Si_3N_4	$2\ HSiCl_3 + H_2SiCl_2$, NH_3 36 g (270 mmol) + 13.5 g (135 mmol); 800 mL THF	$([HSi(NH)_{1.5}]_2(H_2SiNH))]_n$ 18.6 g (128 mmol) 95%	89	

[a] Not determined. [b] Prepared in analogy to ref. 37.

where $\Delta\eta$ is the difference of the scattering length densities $\eta_{p/m} = \rho_{0p/m}\cdot\langle f\rangle_{p/m}$ of the regions p and the matrix m. Using the contrast variation with neutron (n) and X-ray (x) diffraction the relation

$$\frac{Q_x}{Q_n} = \frac{2\pi^2\cdot v_1\cdot(1-v_1)\cdot(\Delta\eta_x)^2}{2\pi^2\cdot v_1\cdot(1-v_1)\cdot(\Delta\eta_n)^2} = \frac{(\Delta\eta_x)^2}{(\Delta\eta_n)^2} \qquad (7)$$

yields a characteristic value for a certain type of regions within a matrix. The left side of eq 7 can be determined from the experiments and the right side of the relation can be calculated for a supposed type of regions. The best agreement of both values provides a criterion for the identification of the type of inhomogeneities in the sample.

3. Experimental Section

3.1. Samples. Polymer synthesis was performed by ammonolysis of di- or trichlorosilanes or mixtures thereof according to the cited references. The synthesis of A3, A5, and A6 is not yet published. Details on the starting compounds used and the polymer structures are given in Table 1. The compositions of the samples derived from these polymers by thermolysis and investigated in the present work are given in Table 2 and are indicated in Figure 1.

Typically, in a three-necked round flask equipped with stirrer, gas inlet tube, and a dry ice/2-propanol reflux condenser, the monomeric starting compounds were dissolved in tetrahydrofuran. After this the mixture was cooled to 0 °C, a moderate stream of ammonia was introduced. In all cases spontaneous precipitation of ammonium chloride occurred. The addition was stopped when ammonia condensation was observed at the reflux condenser. After removing the precipitate by filtration through Celite and evaporating all volatile components by vacuum distillation in a high vacuum at 25 °C, the polymers were obtained as colorless liquids.

Ceramic materials were obtained by bulk thermolysis of the as-obtained precursors at 1050 °C in an Ar atmosphere (heating rate 1 °C/min, holding time 3 h). In addition, samples were annealed at temperatures up to 1500 °C for 16 h in a nitrogen atmosphere in graphite furnaces using graphite crucibles (T < 1050 °C, 10 °C/min; T > 1050 °C, 2 °C/min). For the contrast variation in the neutron scattering experiments two samples with the same intended composition were prepared, sample A2 containing ^{nat}N ($f = 0.936 \times 10^{-12}$ cm) and sample A3 with the isotope ^{15}N ($f = 0.644 \times 10^{-12}$ cm).

Further, one Si−C−N ceramic (B) was produced by sputtering from a SiC target. As substrate, a thin aluminum foil ($d = 50\ \mu$m) on the anode was attached. A portion of nitrogen was added to the sputtering gas argon to receive the desired Si−C−N layer. The sputtering gas argon was injected with a pressure of 7×10^{-3} Torr and nitrogen was injected with a pressure of 9×10^{-3} Torr. This mixing proportion resulted in an amorphous ceramic Si−C−N layer with a composition containing somewhat more nitrogen than precursor-derived ceramics. To receive a substrate-free Si−C−N ceramic powder, the aluminum substrate foil was etched with KOH (10%).

Table 2. Chemical Composition (Weight %; Atom % Given In Parentheses) and Solid State Density ρ of Ceramics A1−A7, B, a-Si_3N_4, and a-C[a]

sample	Si	C	N	formula[b]	x	ρ (g/cm^3)
A1	44.3 (26.9)	25.8 (36.6)	29.9 (36.5)	$Si_3C_{4.08}N_{4.07}$	0	2.26
A2	45.9 (27.8)	31.7 (44.9)	22.4 (27.3)	$Si_3C_{4.85}N_{2.99}$	0.29	2.12
A3	50.7 (31.8)	28.9 (42.5)	20.4 (25.7)	$Si_3C_{4.01}N_{4.07}$	0.48	2.13
A4	37.4 (20.9)	48.6 (63.4)	14.0 (15.7)	$Si_3C_{9.10}N_{2.25}$	0.55	1.84
A5	60.0 (41.4)	14.4 (23.2)	25.6 (35.4)	$Si_3C_{1.68}N_{2.57}$	0.43	2.35
A6	58.6 (40.8)	8.6 (13.8)	32.8 (45.4)	$Si_3C_{1.01}N_{3.34}$	0.17	2.44
A7	58.4 (40.6)	6.4 (10.4)	35.2 (49.0)	$Si_3C_{0.77}N_{3.34}$	0.09	2.52
B	45.9 (28.7)	16.1 (23.6)	38.0 (47.7)	$Si_3C_{2.47}N_{4.99}$		2.62
a-Si_3N_4	60.7 (44.5)	0.0 (0.0)	39.3 (55.5)			2.31
a-C	0.0	100.0	0.0			1.40

[a] Oxygen values are <1 weight % and are omitted. In addition, the thermodynamically calculated values x for the different compositions $Si_{3+(1/4)x}N_{4-x}C_x$ along the tie-line SiC−Si_3N_4 are given. [b] Referring to Si_3.

The solid-state densities (measured with a helium pycnometer) of the investigated precursor-derived ceramics A1−A7, the sputtered ceramic B, and amorphous Si_3N_4 (a-Si_3N_4) are listed in Table 2.

In addition to the amorphous Si−C−N ceramics, a-Si_3N_4 and amorphous carbon (a−C) (Goodfellow, LS214621) were measured with neutron scattering.

Elemental analysis was performed using a combination of different methods. For N and O hot gas extraction in Ni hulls at 2200−2700 °C with a LECO TC 436 N/O analyzer was used. Quantitative determination of N_2 was carried out using a thermal conductivity analyzer. CO_2 (obtained by oxidation of CO that is released during combustion) was determined by IR spectroscopy.[38]

(35) *Product Information VT50*; Höchst AG, Germany.
(36) Huggins, J. Ger. offen. DE 41 14 217 A1, 1992.
(37) Weinmann, M.; Zern, A.; Aldinger, F. *Adv. Mater.* **2001**, *13*, 1704.
(38) Kaiser, G.; Schubert, H. *J. Eur. Ceram. Soc.* **1993**, *11*, 253.

For C, combustion in an Elementar Vario EL, ELTRA CS 800 C/S-analyzer was used. Quantitative CO_2 determination was performed by IR Spectroscopy.

For Si, two methods were used: (a) Atom emission spectroscopy using an ISA JOBIN YVON JY70 Plus instrument, Atom emissions spectrometer. Sample pulping was performed using mixtures of hydrofluoric acid, sulfuric acid, and nitric acid in steel-mantled Teflon reactors.[39] (b) X-ray fluorescence analysis with sequential X-ray spectrometer SRS 303 (Siemens). Sample pulping was performed in Li_3BO_3/B_2O_3.

3.2. Diffraction Experiments and Data Evaluation. X-ray wide-angle scattering was measured up to $q = 20$ Å^{-1} in transmission mode using Ag Kα radiation. From the data, corrected for absorption, polarization, and Compton scattering, the structure factor $S(q)$ was derived according to the Faber−Ziman definition.[31] The neutron wide-angle scattering experiments were performed at the ISIS facility of the Rutherford Appleton Laboratory, U.K., using the SANDALS instrument. With SANDALS a range of the wave vector transfer up to $q = 50$ Å^{-1} could be measured leading to a high resolution in the real space correlation function $G(r)$. For the data correction and the evaluation of the structure factor $S(q)$ the SANDALS program package[40] was used. The incoherent scattering contribution from the hydrogen impurities was subtracted during the data reduction, and the oxygen impurities were neglected, i.e., the samples were treated as a ternary Si−C−N system (for details see ref 29).

The small-angle X-ray scattering (SAXS) experiments were performed with Cu Kα radiation using a pinhole collimation camera equipped with an area detector.[41] Small-angle neutron scattering (SANS) was done at the reactor Orphée of the Laboratoire Léon Brillouin (LLB), CEA, France, using the instruments PAXE and PACE. The SANS experiments were performed over the same q-range as the SAXS measurements (3×10^{-3} Å$^{-1} \le q \le 4.3 \times 10^{-1}$ Å^{-1}). The measured data were corrected for absorption and normalized to absolute units (cm^{-1}) by using a calibrated glassy carbon secondary standard (SAXS) and water (SANS). For details see ref 41.

4. Results and Discussion

4.1. Identification of Atomic Distances. For the identification of contributions of the individual atomic pairs in the amorphous Si−C−N ceramics to the total pair correlation functions $G(r)$, contrast variation by combination of X-rays and neutrons and isotopic substitution was employed. The pair correlation functions $G(r)$ for ceramic A1 measured with both X-ray and neutron scattering and the neutron measurements for ceramics A2 (^{nat}N) and A3 (^{15}N) are shown in Figure 2. Although the resolution in $G(r)$ is worse with X-rays than with neutrons (due to the different q-ranges) it is evident that the contrast variation between X-ray scattering and neutron scattering yields very different pair correlation functions. With X-rays, two distinct peaks at 1.73 and 2.92 Å can be observed (the oscillations between these peaks and in front of the first peak are due to the termination effect), whereas in the neutron $G(r)$ there are four peaks observed at 1.42, 1.73, 2.46, and 2.84 Å. The contrast variation between ^{nat}N and ^{15}N shows a difference in the peak areas of $G(r)$. In combination with the weighting factors W_{ij} (Table 3), the differences can be used for the identification of an individual atomic pair ij, which causes a peak in $G(r)$ (or determines the position of the maximum in case of more than one type of atomic pairs contributing to a peak).

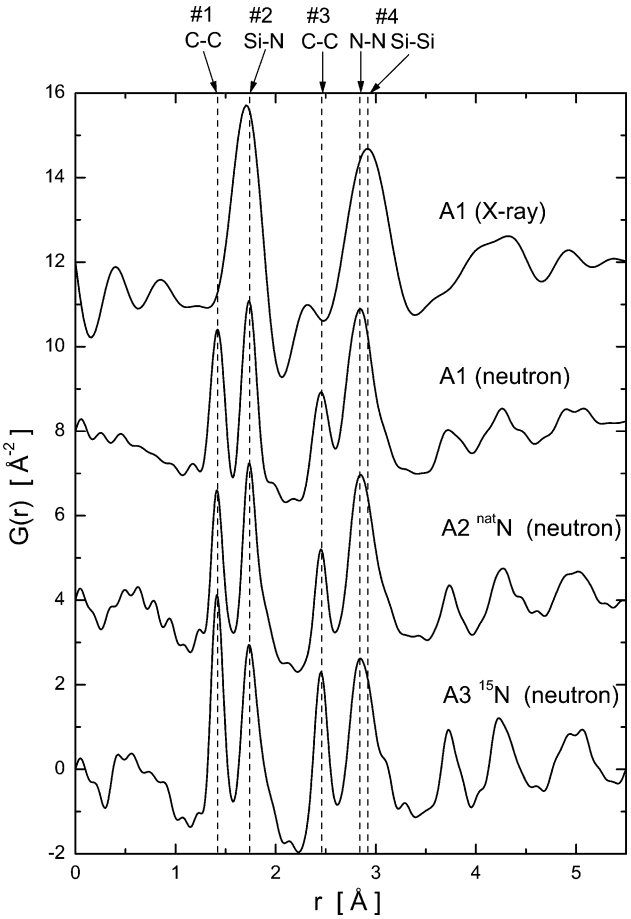

Figure 2. Total pair correlation functions $G(r)$ for Si−C−N ceramics using contrast variation: A1, X-rays ↔ neutrons; A2, A3, ^{nat}N ↔ ^{15}N. The vertical lines indicate the distances in the crystalline phases graphite and α-Si_3N_4.

Table 3. Faber−Ziman Weighting Factors, W_{ij}, for the Ceramic A1 for X-ray (x) (Averaged over q = 0...25 Å) and Neutron (n) Diffraction and for the Ceramics A2 (^{nat}N) and A3 (^{15}N) for Neutron Diffraction[a]

sample		Si−Si	C−C	N−N	Si−C	Si−N	C−N
A1	(x)	0.230	0.056	0.083	0.224	0.272	0.136
A1	(n)	0.026	0.122	0.241	0.112	0.157	0.343
A2 ^{nat}N	(n)	0.030	0.199	0.146	0.154	0.132	0.341
A3 ^{15}N	(n)	0.052	0.237	0.081	0.222	0.130	0.278

[a] The X-ray and neutron scattering lengths were taken from refs 42 and 43.

Peaks 1 and 3. The two peaks at 1.42 and 2.46 Å are not observed with X-rays and thus could be caused by C−C, N−N, or C−N bonds. However, as the peak areas are larger for A3 (^{15}N) than for A2 (^{nat}N) these peaks can be attributed to C−C correlations.

Peak 2. The peak at 1.73 Å appears with X-rays and with neutrons and therefore reflects a Si−N bond. The reduction of the peak area for ceramic A3 (^{15}N) compared to A2 (^{nat}N) supports this.

Peak 4. With neutrons a strong peak is located at 2.84 Å, and because of the larger area for ceramic A2 (^{nat}N) than for A3 (^{15}N), it can be concluded that the main contribution to this peak is due to N−N atomic pairs.

(39) Wörner, W.; Kaiser, G.; Schubert, H. *Mikrochim. Acta* **1993**, *110*, 173.

(40) Soper, A. K.; Howells, W. S.; Hannon, A. C. *Atlas − Analysis of Time-of-Flight Diffraction Data from Liquid and Amorphous Samples;* Technical Report RAL-89-046, Neutron Science Division, Rutherford Appleton Laboratory: Didcot, U.K., 1989.

(41) Härle, J. *Untersuchung schnell abgeschreckter Schnellarbeitsstähle im Bereich grosser und kleiner Impulsüberträge mittels Röntgenstrahlen,* Ph.D. Thesis, Universität Stuttgart, Germany, 1990.

Table 4. Peak Positions in $G(r)$ for all Investigated Amorphous Si−C−N Ceramics, Amorphous Carbon, Amorphous Si_3N_4, and Atomic Distances in the Relevant Crystalline Phases, Graphite,[44] α-Si_3N_4,[45] and SiC[46]

material	peak position r_{ij} (Å) (atomic pair ij)						
A1[a]		1.71				2.92	
A1	1.42	1.74		2.45	2.84		
A2	1.42	1.74	1.90[b]	2.46	2.86		3.11[b]
A3	1.42	1.73	1.89[b]	2.46	2.86		3.14[b]
A4	1.42	1.74	1.89[b]	2.45	2.85		3.15[b]
A5		1.75			2.85		
A6		1.74			2.86		
A7		1.74			2.84		
B	1.42 (C−C)	1.73 (Si−N)	2.00[b] (Si−C)	2.41 (C−C)	2.81 (C−C) (N−N)	(Si−Si)	3.08[b] (Si−Si, C−C)
a-C	1.42 (C−C)			2.46 (C−C)	2.84 (C−C)		
a-Si_3N_4		1.73 (Si−N)			2.84 (N−N)		
graphite	1.42 (C−C)			2.46 (C−C)	2.84 (C−C)		
α−Si_3N_4		1.71, 1.79 (Si−N)		2.58 (N−N)	2.81, 2.94 (N−N)	2.72−3.15 (Si−Si)	
SiC			1.89 (Si−C)				3.06 (C−C) (Si−Si)

[a] A1: from X-ray diffraction. [b] Indicates estimated value.

With X-rays the peak is located at 2.92 Å. According to the W_{ij} factors in Table 3 this distance has to be ascribed to correlations involving Si atoms. Because in case of Si−C or Si−N correlations this distance should be likewise visible with neutron diffraction, it is suggested that the peak maximum at 2.92 Å reflects a Si−Si correlation.

These conclusions from the discussion of the trends observed with total $G(r)$-functions upon contrast variation can be supported by a comparison of the peak positions observed for the amorphous Si−C−N ceramics (A1−A3 in Figure 2) with the atomic distances in relevant crystalline phases (Table 4). The peaks 1 and 3 at 1.42 and 2.46 Å coincide with the C−C distances in graphite, peak 2 at 1.73 Å agrees with the Si−N distances in α-Si_3N_4, peak 4 at 2.84 Å, as measured with neutrons, agrees with the N−N distances in α-Si_3N_4 and with the C−C distance in graphite, and its position at 2.92 Å, as measured with X-rays, falls in the range of Si−Si distances in α-Si_3N_4.

The total structure factors $S(q)$ and pair correlation functions $G(r)$ of all Si−C−N ceramics measured by neutron diffraction are depicted in Figures 3 and 4. If the N/Si ratio is smaller than 4:3, corresponding to Si_3N_4, the peaks at 1.73 and 2.84 Å in the pair correlation functions exhibit an additional shoulder at a larger distance (e.g., A2 and A3 in Figure 4). This is a consequence of the presence of Si−C bonds (in addition to the Si−N bonds) in the amorphous ceramics. This behavior has been found also in a previous study on a $Si_{40}C_{24}N_{36}$ ceramic (N/Si = 0.9), derived from a polyhydromethylsilazane precursor.[22] The values for the atomic distances giving rise to the shoulders were obtained from peak fitting and found to agree with the distances in crystalline SiC (Si−C at 1.89 Å, C−C and Si−Si at 3.06 Å, Table 4). As an example, Figure 5 shows the radial distribution function $RDF(r)$ of the ceramics A1 (Si/N = 3:4) and A2 (Si/N = 1:1) and the decomposition into the individual atomic pairs by Gaussian fitting to the peaks. For the fitting of the $RDF(r)$ of ceramic

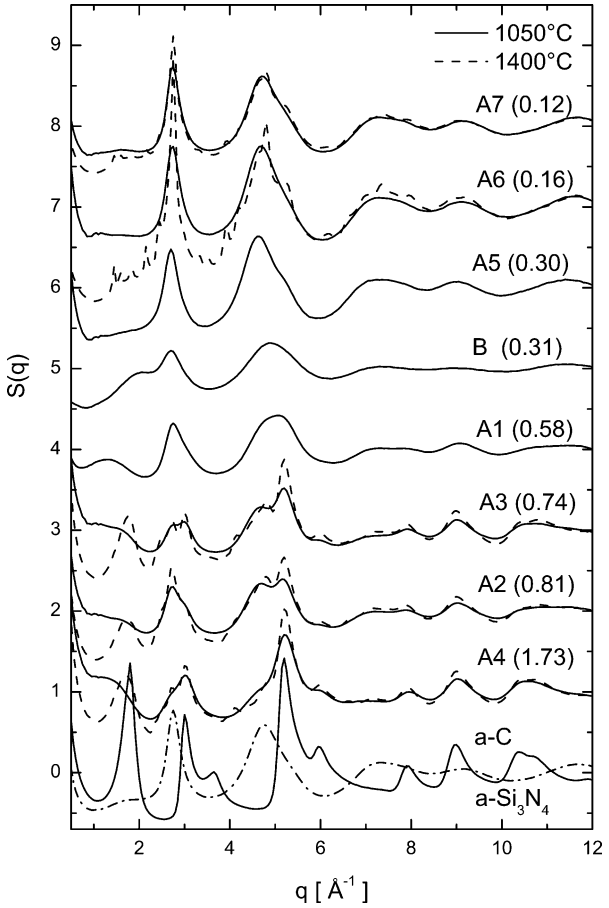

Figure 3. Total neutron structure factors $S(q)$ of the amorphous Si−C−N ceramics with different composition (ratio C/Si_3N_4 is indicated in parentheses) after thermolysis at 1050 °C (—) and after heat treatment at 1400 °C (– – –) and of amorphous carbon (a-C) (—) and of amorphous Si_3N_4 (– · –).

A2 a Si−C contribution at 1.89 Å, in addition to those of C−C and Si−N, is necessary. No further bonds corresponding to atomic distances in SiC were found in the $G(r)$-functions at distances larger than 3.06 Å. Thus,

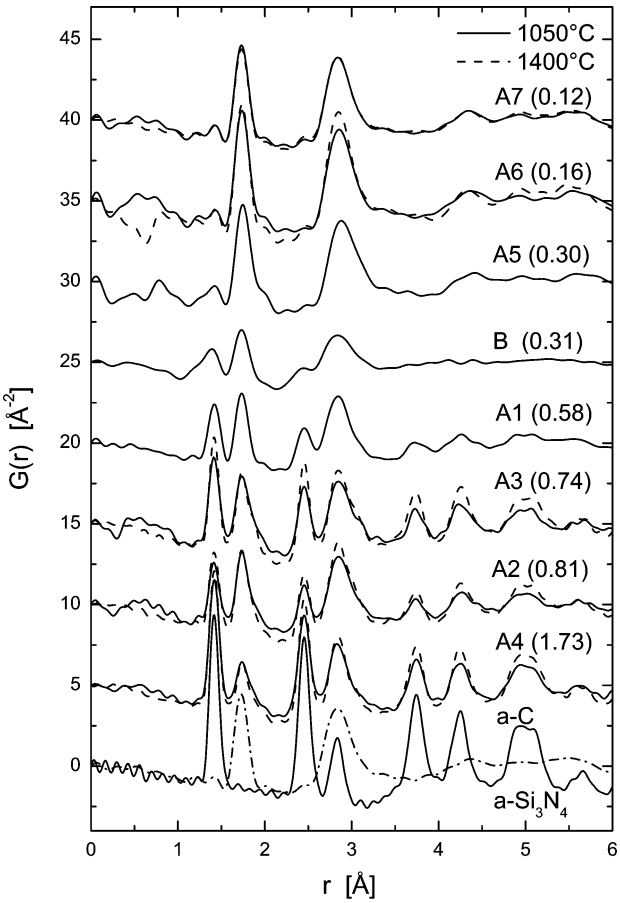

Figure 4. Total neutron pair correlation functions $G(r)$ of the amorphous Si−C−N ceramics with different composition (ratio C/Si_3N_4) after thermolysis at 1050 °C (—) and after heat treatment at 1400 °C (− − −) and of amorphous carbon (a−C) (—) and amorphous Si_3N_4 (− · −).

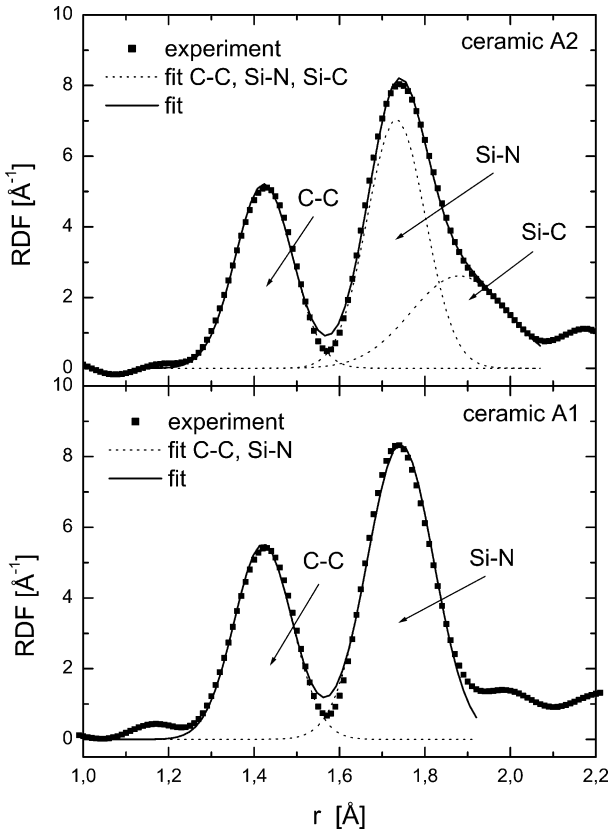

Figure 5. Gaussian fitting of the radial distribution function of the ceramics A1 and A2. For the ceramic A2 an additional contribution from a Si−C correlation was taken into account.

it is suggested that the additional Si−C bonds at 1.89 Å do not belong to a separate amorphous SiC phase but to mixed $Si(C,N)_4$ tetrahedra. This has been found also by means of solid-state NMR measurements.[47] According to this view, part of the C atoms in the ceramics compensate the lack of N atoms if Si/N > 4:3 and the rest of the C atoms are arranged in a graphite-like structure. The N/C ratio of the amorphous phase built by mixed $Si(N,C)_4$ tetrahedra and its composition located on the tie-line Si_3N_4−SiC depend on the overall composition of the ceramic. It can be concluded that the phase composition is (very likely) located on the line Si_3N_4−SiC at the intersection with the metastable tie-line through graphite and the overall composition of the ceramic (e.g., X for ceramic A4 in Figure 1).

4.2. Quantitative Evaluation of the Phase Separation. The structure factors $S(q)$ from neutron scattering for the precursor-derived amorphous Si−C−N ceramics A1−A7, which differ in chemical composition, and the structure factor for the sputtered Si−C−N ceramic B are arranged in Figure 3 according to their C/Si_3N_4 ratio. Additionally, the structure factors of the ceramics A2, A3, A4, A6, and A7 after heat treatment at 1400 °C/16 h are depicted (dashed lines). For comparison, the structure factors of amorphous carbon (- - -) and amorphous Si_3N_4 (- · -) are included.

It is evident that the structure factors of all Si−C−N ceramics are a weighted average of the $S(q)$ functions of a-C and a-Si_3N_4. For example, the ceramics with high carbon content (A2, A3, and A4) show a split of the peaks at $q \approx 3$ Å^{-1} and $q \approx 5$ Å^{-1} into two components which can be attributed to a-C and a-Si_3N_4, respectively. With decreasing C/Si_3N_4 ratio the structure factor converges to that of a-Si_3N_4, and the ceramic A7 with a low C/Si_3N_4 ratio of 0.12 shows a pattern more or less identical to that of a-Si_3N_4. The first broad peak at $q \approx 1.5$ Å^{-1} which is analogous to the (002) reflection in graphite (at $q = 1.85$ Å^{-1}) is shifted toward lower q values. This indicates that the interlayer-distance in amorphous Si−C−N ceramics is larger than that in graphite and also larger than that in a-C ($q = 1.80$ Å^{-1}), and the width of the peak indicates a lower degree of order.

The pair correlation functions $G(r)$ obtained by Fourier transformation of the structure factors in Figure 3 are shown in Figure 4. From the pair correlation functions the same conclusions on phase separation can be drawn as from the structure factors. With decreasing carbon content the contribution from the correlations which belong to the a-C phase becomes lower and finally disappears for the ceramic A7.

Thus, the wide-angle scattering experiments reveal that all the amorphous precursor-derived Si−C−N

(42) Hubbell, J. H.; Veigele, W. J.; Briggs, E. A.; Brown, R. T.; Cromer, D. T.; Howerton, R. J. *J. Phys. Chem. Ref. Data* **1975**, *4*, 471.
(43) Sears, V. F. *Neutron News* **1992**, *3*, 26.
(44) Trucano, P.; Chen, R. *Nature* **1975**, *258*, 136.
(45) Ruddlesden, S. N.; Popper, P. *Acta Crystallogr.* **1958**, *11*, 465.
(46) Shaffer, P. T. B. *Acta Crystallogr.* **1969**, *B25*, 477.
(47) Schuhmacher, J. *Festkörper-NMR−Untersuchungen zur Umwandlung von Polysilazanen und Polysilylcarbodiimiden in Si−(B)-C−N−Keramiken*, Ph.D. Thesis, Universität Stuttgart, Germany, 2000.

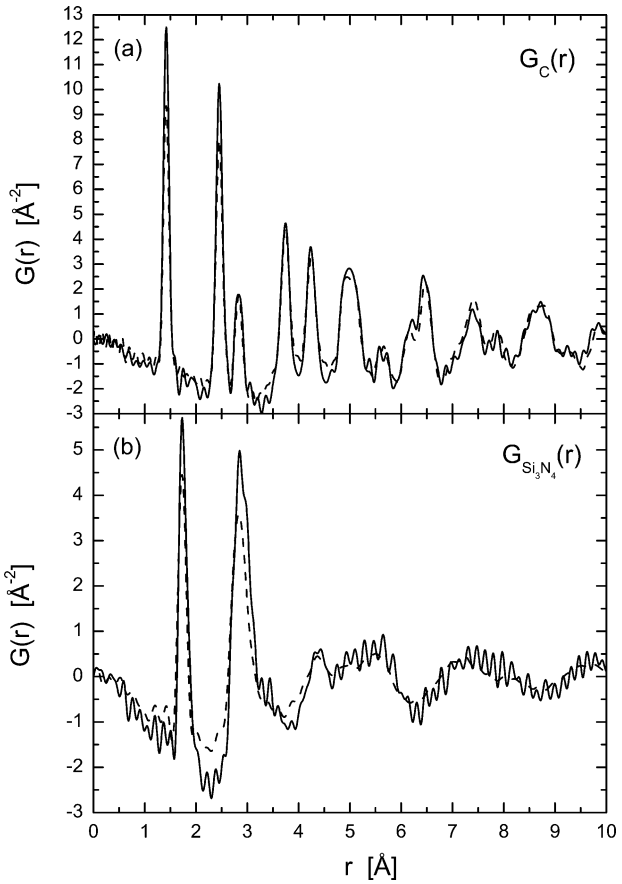

Figure 6. Partial pair correlation functions $G_C(r)$ (a) and $G_{Si_3N_4}(r)$ (b), calculated from the total pair correlation functions of the ceramics A2 and A4 annealed at 1400 °C (—). For comparison the neutron pair correlation functions of the a-C and a-Si_3N_4 samples are also shown (– – –).

ceramics consist of an amorphous graphite-like phase and from amorphous $Si_{3+(1/4)x}N_{4-x}C_x$. Assuming that the structure of these two phases is independent of their relative amounts in the ceramics, their partial structure factors, $S_C(q)$ and $S_{Si_3N_4}(q)$, can be derived from two experiments by the so-called concentration-contrast variation method. This method takes advantage of the different chemical compositions of the ceramics, for example A2 ($C/Si_3N_4 = 0.81$) and A4 ($C/Si_3N_4 = 1.73$), and accordingly different weighting factors of the two separated phases, $W_C = 0.35$, $W_{Si_3N_4} = 0.65$ for A2, and $W_C = 0.53$, $W_{Si_3N_4} = 0.47$ for A4 (The W_{ij} were calculated from the amounts of C and $Si_{3+(1/4)x}N_{4-x}C_x$ constituting the ceramics and the scattering lengths). By the two total structure factors $S(q)$ for A3 and A4 two equations of the type

$$S(q) = W_C \cdot S_C(q) + (1 - W_C) \cdot S_{Si_3N_4}(q) \qquad (8)$$

are provided for calculation of the partial structure factors. Figure 6 shows the partial pair correlation functions resulting from this calculation (and Fourier transformation), where the $S(q)$ of A2 and A4 at 1400 °C have been used in eq 8. The agreement of the calculated partial pair correlation functions $G_C(r)$ and $G_{Si_3N_4}(r)$ with the $G(r)$-functions measured with the samples of amorphous carbon and amorphous Si_3N_4, respectively, presents a quantitative proof for the existence of two separated phases in precursor-derived Si−C−N ceramics.

The existence of regions with short range order similar to that in crystalline Si_3N_4 and regions with a graphite-like structure has been already deduced for a single ceramic, $Si_{24}C_{43}N_{33}$, derived from a polysilylcarbodiimide precursor.[20] Comparison of the pair correlation function $G(r)$ of this ceramic with that of ceramic A1, derived from a polysilazane precursor in the present work (Figure 4), which also lies on the C−Si_3N_4 tie-line with similar composition, shows that the positions and amplitudes of the occurring peaks are identical. This indicates that the general structural features, both short-range order and phase separation, of precursor-derived Si−C−N ceramics do not depend on the type of the employed precursor. However, the Si/C/N composition (see Table 2) and the kinetics of phase separation (as reported in ref 23) are determined by the specific precursor and/or by the details of the production process of the ceramics.

In conclusion of this section it is noted that in ref 20 the existence of Si_3N_4 regions and free carbon has been deduced on the basis of the individual peaks in the pair correlation function $G(r)$ for a single ceramic. In addition to this previous study, from the evaluation of the concentration dependence of the $G(r)$ function in the present work the quantitative separation of the measured $G(r)$ into the partial contributions of the two amorphous phases, Si_3N_4 and carbon, as well as comparison with the structure of amorphous Si_3N_4 and carbon samples, became now possible.

4.3. Relaxation Upon Annealing. After annealing of the ceramics at 1400 °C the structure factors in Figure 3 show a behavior similar to that of the as-thermolyzed samples, but the peaks become sharper indicating an increase of the correlation length in real space. This points to a growth of the phase-separated regions and a decrease in the degree of imperfection of the amorphous structure. For the carbon rich ceramics the separation into two phases becomes more distinct and the first peak at $q \approx 1.5$ Å^{-1}, which corresponds to d_{002} in graphite is shifted to larger values and becomes more pronounced. This is an indication that the order along the *c*-direction in the amorphous carbon phase increases in the Si−C−N ceramics upon annealing and approaches the order present in the pure amorphous carbon sample. The peaks of the pair correlation functions in Figure 4 also become sharper due to an increase of the local atomic ordering upon annealing. These relaxation effects are accompanied by an increase of the density by about 5%. Because of the growth of the two separated amorphous phases the total interface area between them, where local order is less perfect, decreases, and thus the overall observed order and the density increase.

4.4. Structure of the Amorphous Carbon Phase. In the following a detailed investigation of the amorphous carbon phase in the Si−C−N ceramics, based on model calculations, is presented and compared to that of the amorphous (glassy) carbon sample. With respect to this comparison it has to be noted that the structure of amorphous carbon is not unique, but a variety of disordered carbons exists with different degrees of disorder, depending on the method of production (see, e.g., ref 48.) Hence, the specific amorphous carbon sample measured in the present study represents one

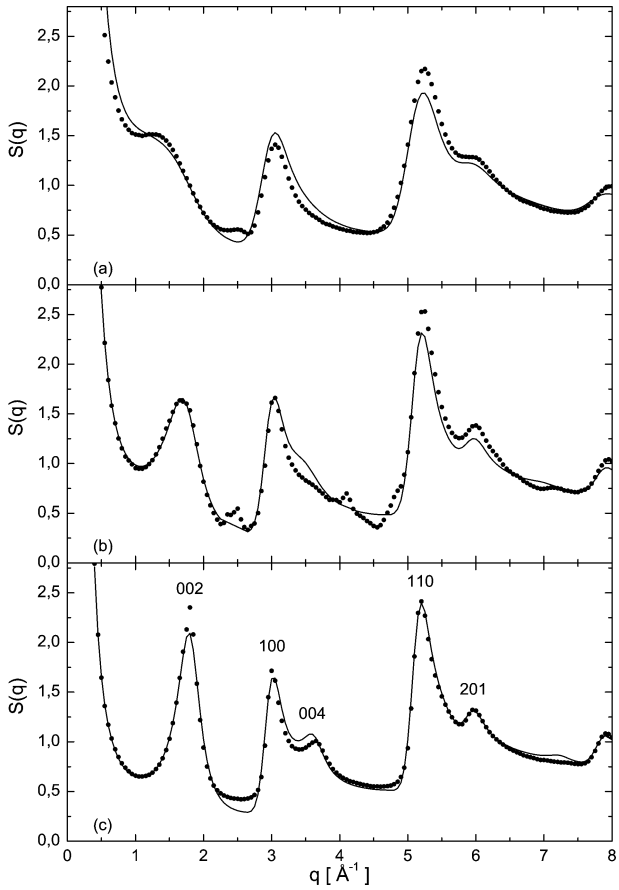

Figure 7. Structure factors $S(q)$ of the amorphous graphite-like phase in Si−C−N ceramics after thermolysis at 1050 °C (a), after additional annealing at 1400 °C (b) and of amorphous carbon (c). The *hkl* are shown for graphite, ··· experimental, − structural model.

of a variety of existing disordered carbons. (Sometimes in the literature the terms amorphous and glassy, respectively, are used to distinguish between three-dimensionally disordered and graphite-like disordered carbons.[49] In the present work these terms are used synonymously.). In Figure 7 the partial structure factors $S_C(q)$ of the amorphous carbon phase in Si−C−N ceramics obtained by the contrast variation method as described in Section 4.2 are shown at thermolysis temperature (a) and after annealing at 1400 °C/16 h (b) together with the $S(q)$ of the amorphous carbon sample (c) (symbols). The structure factor of the amorphous carbon phase in the as-thermolyzed Si−C−N ceramics exhibits less distinct features than the amorphous carbon sample reflecting a more disordered structure. After heat treatment it approaches that of amorphous carbon.

The experimentally derived structure factors were simulated using a structural model for disordered carbon phases as reported in ref 50. The model assumes that the carbon is composed of single-atomic layers of carbon atoms in the graphite honeycomb arrangement, which are then stacked where a certain degree of (turbostratic) disorder is incorporated by adjustable parameters. The structural parameters of the model are as follows: in-plane lattice constant, a; interplanar spacing, $d_{002} = c/2$; lateral size (coherence length) of crystallite, L_a; number of layers in crystallite, M_c; in-plane strain parameter, ϵ_a; fluctuation in spacing between adjacent layers, ϵ_c; probability of random shift between adjacent layers, P_c; and fraction of low-strain regions, g_c.

Table 5. Refined Parameters for the Structure Factor $S(q)$ of the Amorphous Carbon Phase in Si−C−N Ceramics and of Amorphous Carbon (For the Definition of the Parameters see Text)

parameter (units)	Si−C−N 1050 °C	Si−C−N 1400 °C	amorphous carbon
a (Å)	2.46	2.45	2.45
$c/2$ (Å)	3.77	3.60	3.48
L_a (Å)	17.3	22.1	24.3
M_c (n)	8.3	8.0	21.8
ϵ_a (Å)	0.024	0.010	0.007
ϵ_c (Å)	1.95	1.78	1.72
P_c	1	1	1
g_c	0.14	0.38	0.51

The structural parameters were refined by fitting the model structure factors to the experimental ones. The agreement of the simulated and experimental $S(q)$ functions in Figure 7 shows that the disordered carbon phase in Si−C−N ceramics and the amorphous carbon can be well described with the model. The values of the refined parameters are given in Table 5. The in-plane lattice constant (a = 2.45...2.46 Å), which is defined by the covalent bonds, is equal in all three phases. The lateral extension of the layers in Si−C−N ceramics (L_a = 17...22 Å) which is somewhat smaller than that in amorphous carbon (L_a = 24 Å) increases upon annealing. The number of layers (M_c = 8) which corresponds to an extension of 25 Å in c-direction is clearly smaller than that (M_c = 22) in amorphous carbon. Also, the interplanar spacing shows clear differences. The distance decreases from d_{002} = 3.77 Å in the as-thermolyzed ceramic to d_{002} = 3.60 Å in the heat-treated ceramic and thus approximates the value for amorphous carbon, d_{002} = 3.48 Å. The parameters ϵ_a, ϵ_c, P_c, and g_c, which describe the degree of disorder, indicate less order in the amorphous carbon phase in the Si−C−N ceramics than in amorphous carbon. Altogether, it can be stated that the amorphous carbon phase in the Si−C−N ceramics has an in-plane order which corresponds to a large extent to amorphous carbon, but the stacking of the planes in c-direction is clearly less ordered.

The structure of the amorphous carbon phase in a $Si_{24}C_{43}N_{33}$ ceramic and of an amorphous (glassy) carbon sample has been investigated already in a previous study.[20] By using the Reverse Monte Carlo (RMC) method it was possible to generate atomic clusters consistent with the experimental pair correlation functions $G(r)$ and, in particular, to simulate for the Si−C−N ceramic the phase separation into amorphous Si_3N_4 and amorphous carbon. However, it has been suspected[20] that the arrangement of the carbon atoms in the RMC clusters does not fully represent the structure of the real materials: the model clusters did not exhibit two-dimensional order in stacked hexagonal planes, but instead exhibit a three-dimensional amorphous structure and a considerable proportion of the (unlike) bond angle of 60° as compared to the bond angle of 120°. Thus, it is concluded that the structural model for

(48) Robertson, J. *Adv. Phys.* **2001**, *34*, 427.
(49) Li, F.; Lannin, J. S. *Phys. Rev. Lett.* **1990**, *65*, 1905.
(50) Shi, H.; Reimers, J. N.; Dahn, J. R. *J. Appl. Crystallogr.* **1993**, *26*, 827.

disordered carbons where the atomic arrangement in hexagonal planes is incorporated, as adopted in the present work, is better suited for the description of the amorphous carbon phase in amorphous Si−C−N ceramics.

4.5. Sputtered Si−C−N Ceramic. The structure factor $S(q)$ and the pair correlation function $G(r)$ of the sputtered Si−C−N ceramic B are included in Figures 3 and 4. The curves exhibit overall features similar to those of the precursor-derived ceramics and fit quite well into the series of ceramics with increasing ratio C/Si_3N_4. However, regarding the details of the structure factor, differences are also detected. No significant small-angle scattering effect is found (see Section 4.6). The peak at $q \approx 1.8$ Å^{-1} is very broad and is not shifted toward smaller q-values, as observed for the precursor-derived ceramics, but appears at the same position as the corresponding one for amorphous carbon. In the pair correlation function, the first four peaks appear at the same positions as the peaks of the precursor-derived ceramics, but no peaks at r-values greater than 3 Å were observed. This means that the sputtered Si−C−N ceramic has the same atomic short-range order as the corresponding precursor-derived ceramics: the ceramic consists of SiN_4 tetrahedra and rings of carbon atoms which might be also stacked in c-direction. The difference between the sputtered ceramic and the precursor-derived ceramics concerns the medium-range order: there are no phase-separated regions greater than 3 Å. This can be explained by the high cooling rate associated with the sputtering process. The nearest-neighbor arrangement of the deposited atoms is governed by the covalent interaction between the atomic species, independent of the production process, whereas the growth of two separated phases is kinetically hindered due to the low mobility of the sputter-deposited atoms in contrast to the precursor-derived ceramics thermolyzed at 1050 °C.

4.6. Small-Angle Scattering. In this section results from the small-angle scattering experiments are presented for the amorphous Si−C−N ceramic A4. For corresponding results for the ceramics A5 and A6 see ref 29. Figure 8 shows the small-angle X-ray and neutron-scattering cross sections of the amorphous Si−C−N ceramic A4 after thermolysis at 1050 °C and after additional annealing for 16 h at 1200, 1300, 1400, and 1500 °C. It is obvious that the ceramic contains inhomogeneities which cause a signal in the small-angle region. Toward very small q-values the scattered intensities show a linear increase with a slope close to −4 in the log−log plot which is caused by surface scattering from the powder particles according to Porod's law.[51] At larger q-values around $q = 0.1$ Å^{-1} small-angle scattering from the phase-separated regions occurs. With the sputter-deposited ceramic B the latter scattering effect does not occur, proving that this ceramic is homogeneous on the considered medium-range scale.

The scattered intensities strongly depend on the annealing temperature. The shift of the observed scattering effect to lower q-values with increasing temperature indicates that the size of the scattering regions is growing with increasing temperature. The diameter of the regions was determined from Guinier plots, $\ln(d\sigma/d\Omega)$ versus q^2 (cf. Equation 5). With increasing temperature, regions grow from 15 Å at 1050 °C to 30 Å at 1300 °C. Between 1300 and 1400 °C a steplike increase of the scattered intensity (in particular for X-rays, Figure 8(a)) takes place. This is due to the occurrence of traces of Si_3N_4 crystallites in the phase-separated amorphous matrix.[29]

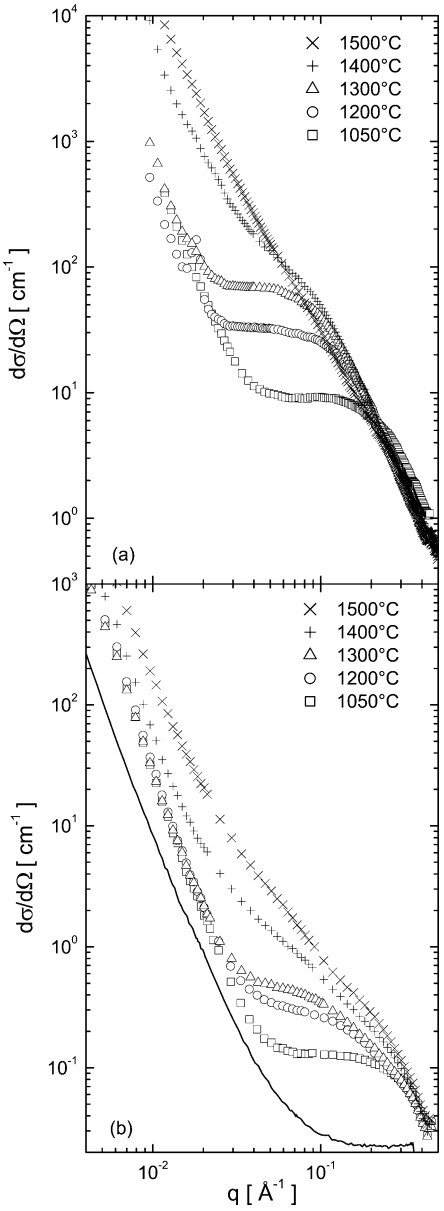

Figure 8. Small-angle X-ray (a) and neutron (b) scattering cross sections of the Si−C−N ceramic A4 after thermolysis at 1050 °C and after annealing at different temperatures for 16 h. The neutron scattering curve (solid line, in arbitrary units) of the sputtered ceramic B is included for comparison.

For the identification of the scattering regions, contrast variation between X-rays and neutrons was employed according to eq 7 following the same procedure as introduced in a previous study.[21] The invariant Q was determined from the experimental cross section after subtraction of the Porod scattering (see above). At large q-values the curve was extrapolated beyond the measured range by using a linear fit (in the log−log plot) to the high-q tail of the measured data. The difference of the scattering length densities of the regions and the

(51) Porod, G. *Kolloid Z.* **1951**, *124*, 83.

Table 6. Diameter (D) of Small-Angle Scattering Regions in the Si−C−N Ceramic A4, Ratio of Invariants $(Q_x/Q_n)^{1/2}$ and Comparison with Calculated Ratios $\Delta\eta_x/\Delta\eta_n$ for Different Types of Inhomogeneities (See Eq 7)[a]

				$\Delta\eta_x/\Delta\eta_n$				
temp. (°C)	D_n (Å)	D_x (Å)	$(Q_x/Q_n)^{1/2}$	pores in Si−C−N	Si_3N_4 in Si−C−N	SiC in Si−C−N	a-C in Si−C−N	$Si_{3+(1/4)x}N_{4-x}C_x$ + C
1050	11.6	16.8	6.1	3.4	5.2	32	1.0	5.0
1200	21.2	28.4	5.3	3.2	5.6	45	1.3	5.3
1300	28.4	36.1	6.1	3.2	5.6	51	1.2	5.4
1400	46.5	43.9	5.9	3.3	5.6	100	0.98	5.3
1500	56.8	51.6	4.6	3.4	5.8	24	0.19	7.0

[a] x: X-rays, n: neutrons. Used number densities ρ_0 for the calculation of the scattering length density η: Si_3N_4, $\rho_0 = 0.103$ Å^{-3}; SiC, $\rho_0 = 0.097$ Å^{-3}; a-C, $\rho_0 = 0.077$ Å^{-3}.

matrix $\Delta\eta$ was calculated for several types of relevant inhomogeneities. In Table 6 the calculated ratios $\Delta\eta_x/\Delta\eta_n$ for X-rays and neutrons are compared with the ratios of the invariants $(Q_x/Q_n)^{1/2}$ as determined from the measured small-angle scattering cross sections. The comparison shows best agreement for two cases: amorphous Si_3N_4 in a matrix phase of Si−C−N, or a system of two separated phases consisting of amorphous $Si_{3+(1/4)x}N_{4-x}C_x$ and amorphous carbon. For the ceramic $Si_{24}C_{43}N_{33}$, lying on the tie-line C−Si_3N_4, phase separation into carbon and Si_3N_4 has been concluded from the contrast variation.[21]

From small-angle scattering alone, a decision regarding which situation is present in the Si−C−N ceramics A4 (apart from the C−Si_3N_4 tie-line) is not possible. Only together with the results from wide-angle scattering, revealing a graphite-like phase and Si−C bonds in addition to Si−N bonds, can the final decision be made that the second case is the real one. Evidently, the combination of both methods, offering their specific merits, provides deeper insight into the structure of amorphous Si−C−N ceramics.

5. Conclusions

Different amorphous Si−C−N ceramics produced by thermolysis of polysilazanes over a wide range of compositions exhibit the same general structural features. They are all separated into two phases. The first is an amorphous phase built by mixed $Si(N,C)_4$ tetrahedra. The N/C ratio of the amorphous phase built by mixed $Si(N,C)_4$ tetrahedra and its composition located on the tie-line Si_3N_4−SiC depend on the overall composition of the ceramic. It can be concluded that the phase composition is (very likely) located on the line Si_3N_4−SiC at the intersection with the metastable tie-line through graphite and the overall composition of the ceramic. The short-range order of this phase is the same as that in amorphous Si_3N_4 and is close to that of crystalline α-Si_3N_4. The second is an amorphous carbon phase with graphite-like short-range order which can be well described by an existing structural model for disordered carbons. The stacking of the hexagonal planes occurs at a larger distance and is less ordered than that of a glassy carbon sample.

The size of the phase-separated regions is about 15 Å. Upon annealing below the crystallization temperature up to 1300 °C for 16 h, the regions grow in size up to about 30 Å and the local structure becomes more ordered. The arrangement of the stacked layers in the amorphous carbon phase approaches the order in glassy carbon.

A Si−C−N ceramic produced by sputter deposition has the same atomic short-range order as the corresponding precursor-derived ceramics but there are no phase-separated regions greater than 3 Å.

The combination of complementary methods, X-ray and neutron diffraction in the wide-angle and in the small-angle ranges, is essential for the investigation of the structure of amorphous Si−C−N ceramics.

Acknowledgment. This work was supported by the Deutsche Forschungsgemeinschaft through grant La 686/3-2. We appreciate the help of Dr. Luec Auvray (LLB, Saclay, France) during the neutron small-angle diffraction experiments and of Dr. Chris Benmore (ISIS, Didcot, UK) during the neutron wide-angle diffraction experiments.

CM031029F